J Solid State Electrochem (2011) 15:1631–1646
DOI 10.1007/s10008-011-1453-1

REVIEW

Recent Advances in in situ multi-spectroelectrochemistry

Lothar Dunsch

Received: 26 April 2011 / Revised: 15 May 2011 / Accepted: 16 May 2011 / Published online: 23 June 2011

Abstract To consider the past, present and future of in situ spectroelectrochemistry, a review on the recent state of modern spectroelectrochemistry and trends in the development of spectroelectrochemcial techniques is presented for the combined application of different in situ spectroelectrochemcial methods like ESR spectroelectrochemistry, NMR spectroelectrochemistry, Raman spectroelectrochemistry or IR spectroelectrochemistry to electrode systems. Starting with a discussion of the first steps in spectroelectrochemistry in the past, the main part of this review is focused on the advantages of the combined application of spectroelectrochemical techniques in the analysis of electrode reactions. The spectroelectrochemical methods are demonstrated to be successful in electrode reactions both for solid structures like polymers or carbon nanotubes and for molecular structures like fullerenes and oligothiophenes. The final outlook is attributed to future developments in spectroelectrochemistry.

Keywords in situ spectroelectrochemistry · Cyclic voltammetry · ESR spectroscopy · NMR spectroscopy · Raman spectroscopy · IR spectroscopy · UV–vis NIR spectroscopy

L. Dunsch (✉)
Center of Spectroelectrochemistry, Department of Electrochemistry and Conducting Polymers, IFW Dresden, Helmholtzstrasse 20,
D-01069 Dresden, Germany
e-mail: l.dunsch@ifw-dresden.de

Introduction

Among the more than 3,000 papers published within the last decade in the field of spectroelectrochemistry, a diversification of the spectroscopic methods applied in electrochemical research is obvious. Based on modern developments in spectroscopic techniques, the combination of electrochemical and spectroscopic techniques is getting more reliable and the performance of sensitive spectroscopic measurements under well-controlled electrode potential conditions accessible. This is the field of in situ spectroelectrochemistry which embraces all spectroscopic measurements at a working electrode under electron transfer. In this way, the drawback of ex situ methods with a spectroscopic characterisation of the electrode reaction products far from the electrochemical cells and without an applied electrode potential is avoided. In ex situ methods, changes of the subject of electrochemical reaction under

study will cause misinterpretations of the real situation at the electrode. To study intermediates in electrode reactions, the in situ spectroelectrochemical methods are the matter of choice to get reliable results in time-dependent studies at selected electrochemical conditions. The use of spectroscopic methods in electrochemistry is caused by the main drawback of all electrochemical methods. Although we have a large variety of electrochemical methods at hand [1–6], there is no way to get any structural information of the electrode system besides the detailed knowledge of charge transfer, transport and distribution. As far as some metal ions with a preferred redox state and their transformation into the metallic state are studied, a clear description of the chemical entity might be possible from electrochemical data. But for metal ions with mixed redox states (in solution or in the solid phase), metal complexes (with redox active ligands) or organic structures, the matter of a charge-transfer reaction is more complex, and a conclusion of some intermediate states, like radicals from the number of transferred electrons, ends up in speculation. As modern electrochemistry is focused on electrode reaction mechanisms, there is no other way than spectroelectrochemistry to get a qualified picture of the state-of-the-art in electrochemical reactions.

It turns out that the spectroscopic methods are applied both to the solid [7] and to the liquid phase [8] of the electrode. Due to their specific interaction with the subjects under study, some spectroscopic methods are applicable for both phases of an electrode, while other methods are preferred for a single phase and its characterisation. IUPAC commission has summarised all spectroscopic methods applied in electrochemistry resulting in a tremendous variety of methods [9]. Nevertheless, there are some spectroscopic methods which are preferred in their use in spectroelectrochemistry. Astonishingly, it is not the importance of a spectroscopic method responsible for the access of important structural data in an electron-transfer reaction in experimental studies, but in most cases, the ease of application (or the technical preference of the leading author) is dominating the choice of the method. Otherwise, there would be a predominance of in situ electron spin resonance (ESR) spectroelectrochemistry in the study of elementary reactions in the electron transfer. In a simple consideration of the both components of a single-electron transfer, one of these has an odd number of electrons. Thus, the unpaired electron might be accessible to ESR spectroscopy, and at least one component might be characterised by this method (no doubt that the electron distribution in chemical species is often more complex). But the availability of the ESR technique to most of the electrochemical laboratories and the requirements in the setup for electrochemical systems restricted the application of this method very often. Therefore, UV/vis spectroscopy is the most applied method in spectroelectrochemistry irrespective of the fact that other methods would result in more detailed structural information.

There have been some monographs in the field [10–18], but a modern extended overview of the most important spectroelectrochemical methods is still missing. Among all presentations of spectroelectrochemical techniques, the role of radiation in the reactions at electrodes is often not considered but should be mentioned. This is the bridge to photoelectrochemistry which is not the subject of the presentation.

The past

Although there is an extended number of papers in spectroelectrochemistry since a first attempt in 1946 [19] with ellipsometry until the end of the 1960s, the term ‘spectroelectrochemistry’ was introduced by Kuwana [20] in 1969 who pushed the field forward based on the activities in the Adams group since 1962. Astonishingly, it was already in 1958 when a wave of in situ ESR spectroelectrochemical studies was initiated [21, 22]. At that time, the new spectroelectrochemical technique was attractive for both fields: in electrochemistry, it was a matter of choice to characterise the products of a primary electrode reaction especially of organic structures. Therefore, the growth of organic electrochemistry in the 1960s pushed the studies in ESR spectroelectrochemistry forward. On the other side, ESR spectroscopists used the electrochemical methods for generation of radicals, the structure of which was of high importance. As far as the electrode reactions (and the molecular structures) were quite simple, the field was attractive for both sides. As more complex situations were to be studied, the ESR spectroscopists lost their interest in the electrochemical method, while electrochemists started to improve the experimental setup for a detailed potential control of the working electrode [23].

The field of spectroelectrochemistry was broadened in the 1960s by the introduction of optically transparent electrodes [24] in 1964 for absorption spectroscopy in transmission, the introduction to the attenuated total reflection (ATR) technique [25] and the use of thin layer cells [26] for IR spectroelectrochemistry in 1968. A breakthrough in Raman spectroelectrochemistry was the discovery of surface-enhanced Raman pattern at silver electrodes [27]. Together with the availability of the laser Raman technique, this vibrational spectroscopy was since then a standard method in in situ spectroelectrochemistry. NMR spectroelectrochemistry of molecular structures was made accessible in 1975 by a spinning cell construction [28] to get well-resolved NMR spectra. It took the NMR

technique three more decades to have the quality of probe heads at such a level to require no longer a spinning of the cell for quality improvements what allowed the construction of a more suitable in situ NMR cell with high sensitivity for a broad range of in situ NMR spectroelectrochemical studies [29]. Furthermore, in situ X-ray diffraction was made reliable with the cell construction [30] for Bragg-type measurements and a special cell [31] for studies of metal monolayers.

With this short presentation, the historical scheme of modern spectroelectrochemcial methods, we considered the background of modern spectroelectrochemistry. It is by no means complete in the listing of all important papers in the field which goes beyond the scope of this paper like a description of all special methods used in spectroelectrochemistry.

The present

Modern research in spectroelectrochemistry is characterised by a combination of different spectroscopic methods for a detailed study of electrode reaction mechanisms or complex electrode systems. Considering the reaction of a neutral organic redox system, it was stated already in the introduction that the primary cathodic or anodic electron transfer would result in an ion radical. The spectroscopic method of choice is ESR spectroscopy to prove the existence of a paramagnetic structure. But either a second electron transfer or chemical follow-up reactions of the radical can result in diamagnetic structures which are not detectable by ESR. Therefore, at least one additional spectroscopic method is required to detect the diamagnetic intermediates and reaction products. The development of an optical ESR cavity opened the route to a simultaneous application of both ESR and UV–vis NIR spectroscopy in a single in situ spectroelectrochemical technique [32] (triple method) for studies at the same working electrode. In this way, both the paramagnetic and diamagnetic structures can be followed in electrode reactions at the same working electrode. But the absorption spectra of diamagnetic structures are overlapping in mixtures of intermediates and/or products, and UV–vis NIR spectroscopy generally suffers from fairly low resolution. Therefore, other spectroscopic methods resulting in more detailed structural information have to be applied (at least in parallel). Among the candidates, FTIR spectroscopy is the most spread method and based on effective cell constructions [33], while NMR spectroscopy is unbeatable in structural details of molecules and solids but suffers from low applicability which was bypassed with new technical standards [29] recently. Furthermore, Raman spectroelectrochemistry turned out to be a powerful tool especially in the study of charging (doping) of carbon nanostructures [34, 35].

For all spectroscopic methods listed here, some experimental studies are given. Furthermore, the following presentation of experimental results in combined in situ spectroelectrochemistry will deliver examples of electrode reactions both in solution and in the solid state.

Spectroelectrochemistry of organic molecules in solution

As a first example, an oligothiophene is presented, which is a material attractive for organic electronics. As the type, number and position of substituents and the number of monomers in oligothiophenes can influence both the stabilisation of charged states as well as the solubility the recently prepared 5,5″-dicyano-3,3″-dibutyl-2,2′:5′,2″:5″,2″-quarterthiophene (DCNDBQT) was used for studies in solution [35] (Scheme 1), as the alkyl side chains result in sufficient solubility on organic solvents, while the electron-acceptor cyano group promotes reduction processes.

The cyclic voltammetry of DCNDBQT (Fig. 1) points to a two-step oxidation (a first reversible and an irreversible second one) and a single reduction step. The reversibility of the second oxidation under formation of the dication can be shown (Fig. 1) by cyclic voltammetry at higher scan rates (100 Vs^{-1}) The first oxidation and reduction processes should result in radical ions which are to be followed by in situ ESR UV–vis NIR spectroelectrochemical analysis. Figure 2 shows the UV–vis NIR spectra during the first electron transfer in the anodic (Fig. 2a) and cathodic (Fig. 2b) range. The two bands at 646 and 1,050 nm for $DCNDBQT^{+\bullet}$ are assigned to SOMO–LUMO and HOMO–SOMO transitions, respectively, while for $DCNDBQT^{-\bullet}$, the bands at 752 and 1,506 nm can be assigned to HOMO–SOMO and SOMO–LUMO transitions, respectively (Fig. 2b).

Direct evidence for the radical species of DCNDBQT was supplied by ESR spectroelectrochemistry. The ESR spectrum of the cation radical $DCNDBQT^{+\bullet}$ (g=2.0025) is given in Fig. 3a, while Fig. 3b presents the ESR spectrum of the anion radical $DCNDBQT^{-\bullet}$ (g=2.0042). Potential dependent ESR measurements underline the reversible formation of both radicals, the g-factors of which differ significantly. The

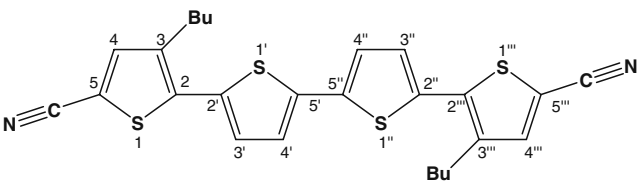

Scheme 1 Chemical structure of 5,5″-dicyano-3,3″-dibutyl-2,2′:5′,2″:5″,2″-quaterthiophene (DCNDBQT)

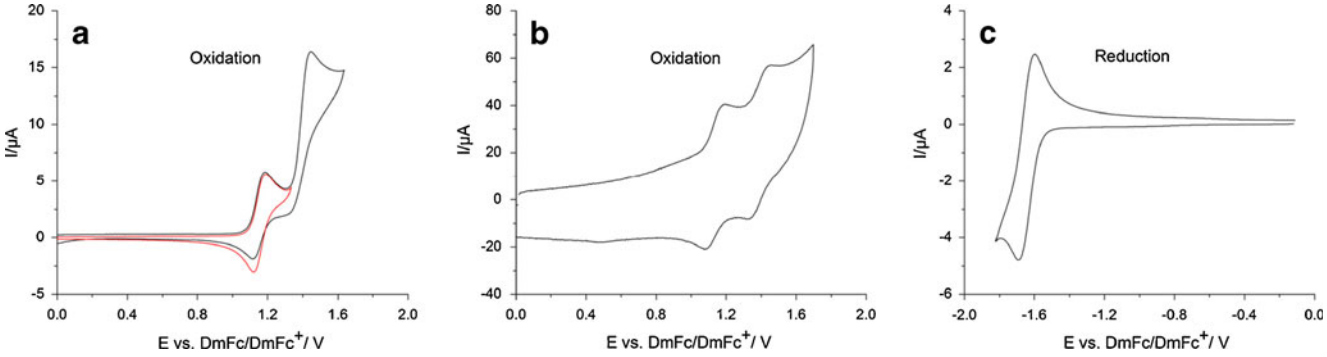

Fig. 1 Cyclic voltammograms of DCNDBQT in ACN/$TBAPF_6$; **a** oxidation, *red*—first oxidation step, *black*—first and second oxidation steps, scan rate 0.05 V/s; **b** oxidation, scan rate 100 V/s **c** reduction, scan rate: 0.05 V/s. (concentration 0.0005 mol/l, working electrode, platinum wire) [37]

first value is close to the g-factor of the free electron (2.0023). The following hyperfine splitting constants were obtained for the cation radical: $a(2H_{23,26})$=0.2752 mT (0.1778 mT), $a(2H_{24,25})$=0.2056 mT (0.1549 mT), $a(2H_{32,35})$=0.0905 mT (0.0857 mT), $a(2H_{33,36})$=0.1959 mT (0.1121 mT), $a(2H_{22,28})$=0.0172 mT (0.0151 mT) and $a(2\ N_{55,56})$=0.0321 mT (0.0233 mT). The hyperfine splitting constants of the $DCNDBQT^{-\bullet}$ radical are: $a(2H_{23,26})$= 0.1308 mT (0.0928 mT), $a(2H_{24,25})$=0.0222 mT (0.0172 mT), $a(2H_{32,35})$=0.0429 mT (0.0395 mT), $a(2H_{33,36})$=0.1659 mT (0.1023 mT), $a(2H_{22,28})$=0.001 mT (0.0014 mT) and $a(2\ N_{55,56})$=0.0560 mT (0.0402 mT).

By quantitative ESR analysis of the redox process, the ratio of the charge transferred to the spin number for the cation radical was determined to be 2.1. Obviously, less than 50% of the charge result in a stable radical formation (for the anion radical, this ratio is even higher—3.0). The

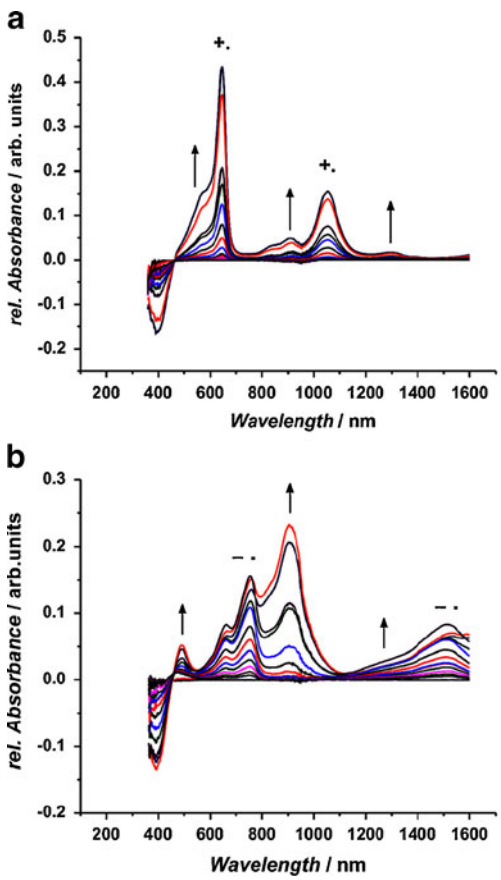

Fig. 2 UV–vis NIR spectrolectrochemistry at the first **a** oxidation and **b** reduction step of DCNDBQT (c=0.0001 M) in 0.1 M $TBAPF_6/CH_3CN$ electrolyte solution [36]

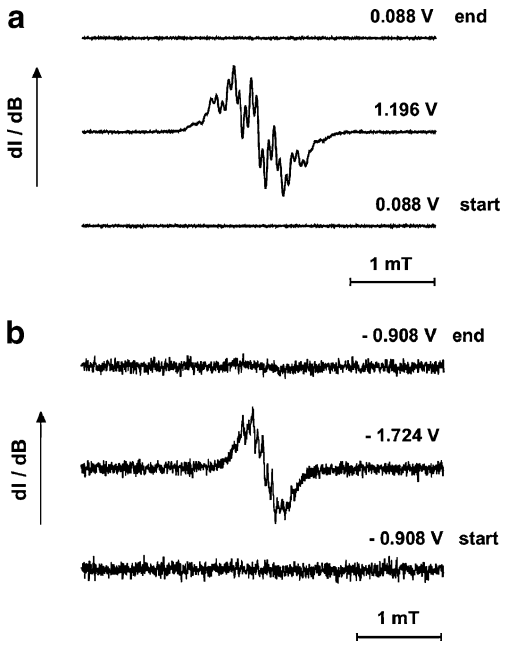

Fig. 3 ESR spectroelectrochemistry of DCNDBQT in 0.1 M $TBAPF_6/CH_3CN$ under potentiostatic control at **a** anodic and **b** cathodic potentials (vs. $DmFc/DmFc^+$ redox couple) (accumulation of 20 spectra) [36]

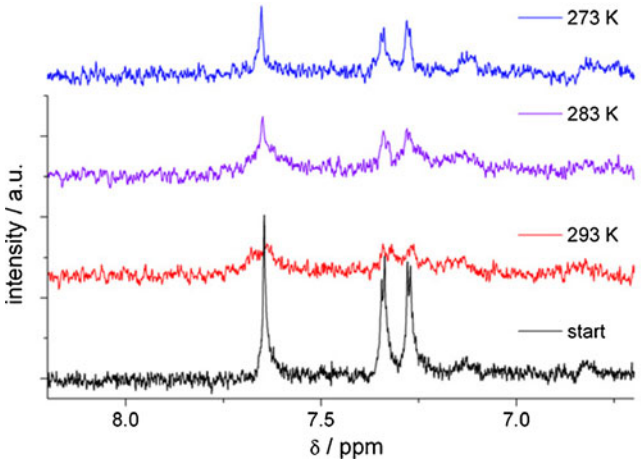

Fig. 4 In situ ^{1}H-NMR spectroelectrochemistry of DCNDBQT in acetonitrile/TBAPF$_6$ at an electrode potential of 1.19 V (working electrode—carbon fibre) at three different temperatures [37]

diamagnetic structures formed are expected to be caused by dimerisation, but the type of dimerisation is to be clarified.

By in situ NMR spectroelectrochemistry [37], the dimerisations in both the first oxidation and the reduction steps were followed under potentiostatic electrolysis. Starting with the first oxidation peak at 1,190 mV, the NMR proton signal (Fig. 4, first line) decreases during electrolysis to zero after 3 h of electrolysis (Fig. 4, second line). This decrease is caused by the formation of the paramagnetic radical which is not detectable in NMR. By temperature-dependent in situ NMR spectroelectrochemical measurements (Fig. 4, third and fourth line), a signal appears at 283 and 273 K shifted by 0.1 ppm to lower field. This signal can be attributed to the diamagnetic π-dimer of the monocation radical of DCNDBQT. The slight shift of the signal to lower field is due to the lower electron density of the oxidised molecule.

Furthermore, the second anodic electron transfer of DCNDBQT was studied by in situ NMR spectroelectrochemistry as well (Fig. 5). The NMR spectrum in CD_2Cl_2 solution with TBAPF$_6$ as supporting electrolyte shows signals of three doublets and four singlets (Fig. 5). This pattern can be attributed to a dimer formed by σ-bond formation between two thiophene rings in 4′ position. Although the oligothiophene is end-capped by CN groups, the doubly charged DCNDBQT dimerises as the four thiophene rings cannot stabilise two positive charges (Scheme 2). The dimerisation is not reversible in re-reduction. The existence of the dimer of the dication was also proved by ex situ MALDI TOF mass spectrometry after extended electrolysis.

The quasi-reversible redox peak of DCNDBQT at −1,680 mV results to a lower extent in an anion radical as shown by quantitative ESR spectroelectrochemistry. The in situ NMR spectroelectrochemical experiment results only in a decrease of the signal intensity during electrolysis at −1,680 mV, but no additional signals arise in the NMR spectrum. After electrolysis, a dark-coloured precipitate is observed in the spectroelectrochemical cell which was analysed by ex situ MALDI-TOF mass spectrometry. As higher mass peaks above 1,476 m/e were found pointing to a trimer, the formation of insoluble polymeric structures by follow-up reactions of the anion radical is demonstrated. As a summary of all spectroelectrochemical studies applied with different methods, the complete reaction mechanism of DCNDBQT under oxidation (as well as reduction) was clarified (Scheme 2).

Spectroelectrochemistry of solid structures at electrodes: the conducting polymers

The spectroelectrochemistry of solid structures at electrodes is preferably to be studied by in situ ESR UV–vis NIR spectroelectrochemistry, and the long story of polyaniline (PANI) still requires further work to follow the influence of the chemical structure on the redox reactions of the polymer. Especially the role of phenazine structures (Fig. 6) in the stabilisation of charged states in PANI is of interest for the use of differently prepared PANI. Therefore, electrochemically prepared PANI and the copolymers of aniline and a phenazine derivative (3,7-diamino-5-phenyl-

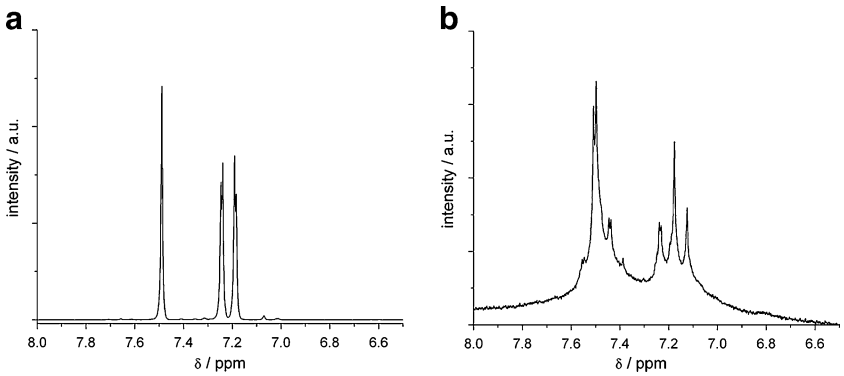

Fig. 5 ^{1}H-NMR spectra of the monomer DCNDBQT (**a**) and its dimer (**b**) (only aromatic range is shown) at the second anodic oxidation step [37]

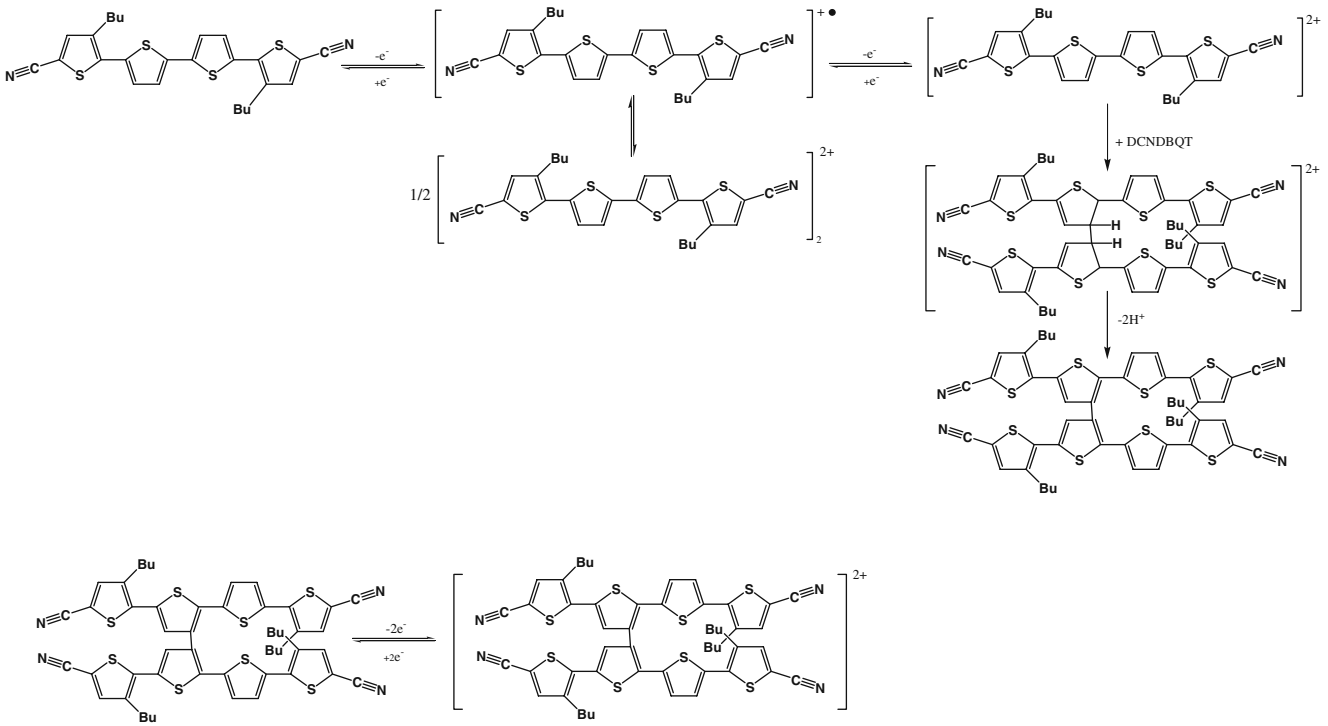

Scheme 2 Mechanism of the oxidation of DCNDBQT including the chemical follow-up reactions via π- and σ-dimer formation [37]

phenazinium chloride, phenosafranine) were compared in their spectroelectrochemical behaviour [38].

For the detailed study of charged states in conducting polymers, it is of high importance that the existence of a polaron pair and that of a polaron can be differentiated by in situ ESR UV/vis NIR spectroelectrochemistry, and their electrode potential-dependent formation is available now to give new insights in the formation of these charged states in PANI. Therefore, the formation of charged states in PANI and aniline–phenosafranine copolymers upon oxidation was followed by in situ ESR UV–vis NIR spectroelectrochemistry. The ESR response of PANI and the copolymers during a voltammetric scan is presented in Fig. 7a. Here, a reversible polaron formation in the forward and back scan is detected. The ESR spectra of both PANI and the aniline–phenosafranine copolymers in the doped state are very similar and have a narrow ESR signal with linewidth of 0.5 G (Fig. 7b) which is unchanged during the voltammetric scan, while polyphenosafranine gives no ESR signal upon oxidation or reduction. Obviously, some extent of a linear chain is required to stabilise a polaron, but the extent of the phenazine content in the copolymer does not have any influence on the polaron behaviour. Contrarily, the potential dependence of the ESR intensity of the copolymer 3, with a higher portion of phenosafranine, differs from that of PANI for equal charges injected into the polymer layer (Fig. 7c). Therefore, the potential dependence of the formation of charged states requires a further detailed study.

The potential dependence of the polaron formation in PANI and the phenazine copolymer (Fig. 8) points to a potential difference between the half-peak current and the ESR intensity (as the signal of the polaron) of 70–80 mV. Therefore, the formation of the polaron is potential-delayed. It is the rare case for PANI that the polaron is not the primarily formed charged state at the polymer chain, but at first, the polaron pair is formed by a two electron transfer

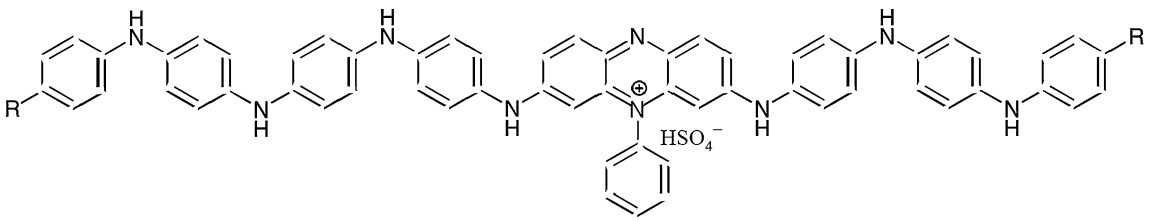

Fig. 6 Chemical structure of a linear polyaniline with a phenazine unit

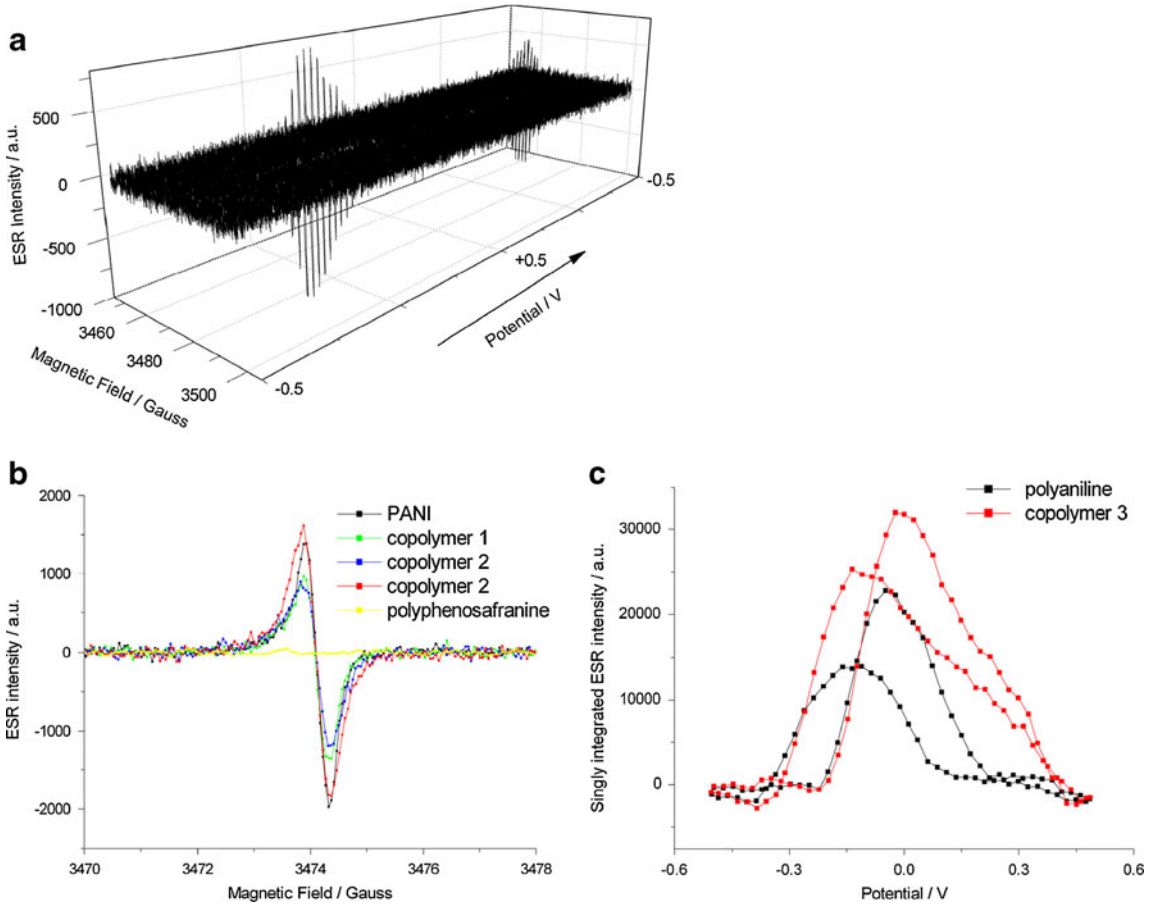

Fig. 7 **a** The potential dependence of the ESR signal of the copolymer 2 during the voltammetric scan in aqueous solution of 0.1 M sulphuric acid and 0.01 M sodium p-toluenesulfonate. **b** ESR signal of PANI, the different copolymers and polyphenosafranine in the doped state. **c** Potential dependence of integrated ESR intensity of PANI and the copolymer 3 [38]

which can dissociate into two polarons at higher potentials. The absorption peaks of the polaron might be hidden by the absorption of the polaron pairs, but the existence of the polaron can be clearly proved by the simultaneous ESR

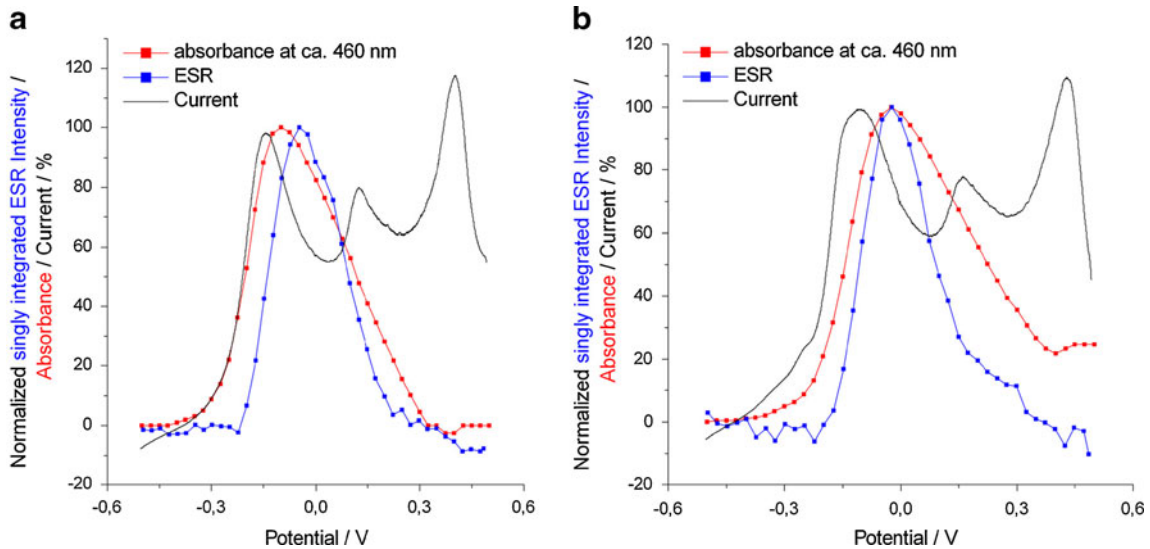

Fig. 8 Potential dependence of the current, the ESR intensity and the absorbance at approximately 460 nm of polyaniline (**a**) and a phenazine/aniline copolymer (**b**) normalized to the maximum of the ESR intensity [39]

measurements. Due to the shift of the maximum of the polaron formation from the peak current, it is to be concluded that the polaron can be formed both by oxidation of the neutral polymer at higher potentials and by dissociation of the polaron pair at the lower potential range. The mechanism for the formation of the charged states in PANI upon oxidation includes an early step in the charge injection as the polaron pair formation.

To analyse the role and charging behaviour of the phenazine unit in PANI, the p-doping of PANI was studied in addition to ESR by in situ ATR-FTIR spectroelectrochemistry [39]. At first, by FTIR spectra of as-prepared polymers as well as in situ FTIR spectra during the oxidation of the polymers, clear evidence for the presence of phenazine-like units in the structure of electrochemically prepared PANI is given, as shown by vibrations of the phenazine rings.

The in situ FTIR spectra measured during the oxidation of PANI are given in Fig. 9. The increase of the IR absorption above 1,700 cm^{-1} is related to the presence of free charge carriers, while the decrease in the IR band around 1,510 cm^{-1} caused the benzoid ring mode to indicate a loss of the benzoid ring structure which is transferred into semiquinoid or quinoid structures. During p-doping, the in situ FTIR spectra with the characteristic vibrations of linear structures are observed together with a new peak at 1,540 cm^{-1} attributed to the changes induced in the phenazine-like units. The IR peaks at 1,572, 1,476, 1,318, 1,250 and 1,145 cm^{-1} appear at higher potentials than the polaron formation and correspond to doubly charged states in the polymer such as the π-dimers.

Therefore, the detailed analysis of the different FTIR spectra give evidence of the existence of phenazine-like units in polyaniline. By the potential dependence of the IR band at 1,540 cm^{-1} and the NIR absorption at 1,500 nm, it was shown that the part of π-dimers in the polymer is stabilised at the link of the phenazine unit to the linear PANI segment, while the linear aniline segment stabilises the polaron and the polaron pair in the PANI structure in the initial oxidation. Two peaks at 1,630 and 1,375 cm^{-1} observed at high electrode potentials are attributed to the bipolaron in PANI.

Spectroelectrochemistry of composed solid structures at electrodes: carbon nanostructures and conducting polymers

The combination of in situ spectroelectrochemical methods is advantageous in the case of composites of polymer/carbon nanostructures, as selective spectroscopic methods can be applied for each component of the composite. Thus, for composites of carbon nanotubes and polymers/oligomers, in situ ESR spectroelectrochemistry is the

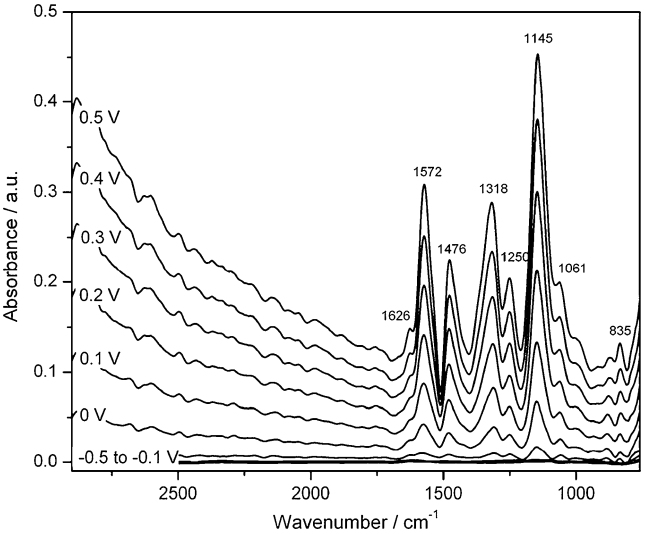

Fig. 9 In situ ATR-FTIR spectroelectrochemical study of the anodic oxidation of PANI at potentials between −0.5 and 0.5 V at a scan rate of 1 mV s^{-1}. Spectra were taken at each 0.1 V and correspond to a potential range of 0.09 V. Reference spectrum taken at −0.5 V [39]

method to characterise the charge-injected changes in the organic component [40], while Raman spectroelectrochemistry [34, 35] is the method of choice for a sensitive evaluation of charged-induced changes in the carbon nanostructure [41] influenced by the interaction with the polymer/oligomer.

The in situ ESR UV–vis NIR spectroelectrochemical study of the oligothiophene/single-walled carbon nanotube (SWCNT) interphase shows for β,β′-dihexylsexithiophene (β,β′-DHST) two reversible redox steps. An ESR signal of the oligothiphene cation radical is detected at the first oxidation step (Fig. 10). The increased voltammetric current (not shown) of the composite results astonishingly

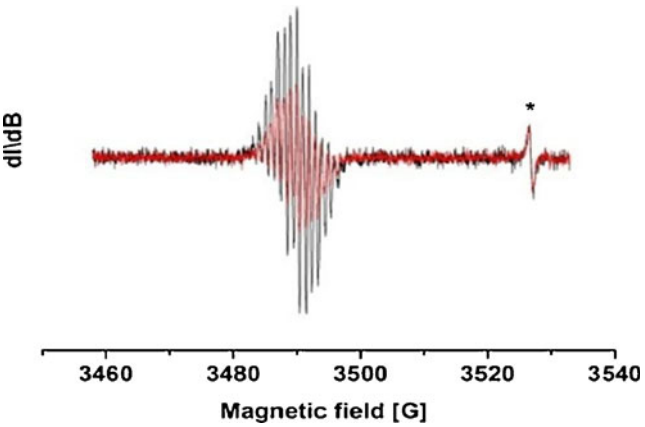

Fig. 10 ESR spectroelectrochemistry of β,β′- dihexylsexithiophene (β,β′-DHST) cation radical in the absence (*black line*) and the presence of SWCNT (*red line*) in 0.1 M $TBAPF_6/CH_2Cl_2$ (*ESR line of Mn^{2+}) [40]

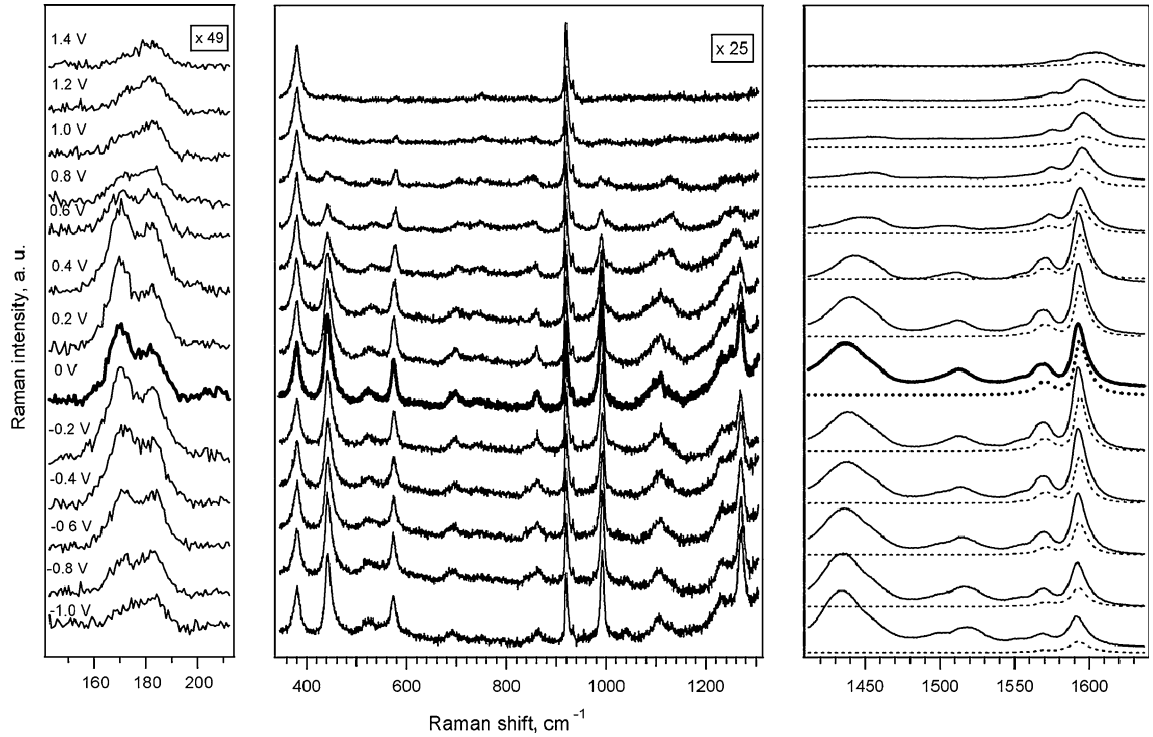

Fig. 11 Potential dependent Raman spectra (excited at 2.54 eV) of SWCNT–PEDOT/PSS composites (*solid lines*) and pristine SWCNT (*dotted lines*) on a Pt electrode in 0.2 M $LiClO_4$/acetonitrile. The electrode potential varied by steps of 0.2 V from 1.4 to −1.0 V vs. Ag pseudoreference electrode for curves from top to bottom. Spectra are offset for clarity. The spectra of pristine SWCNT are scaled by a factor of 0.3 for clarity [41]

in a decreased cation radical concentration (Fig. 10, red signal). This decrease of the ESR signal (and of the radical concentration) can be explained by a π-dimerization of this oligothiophene radical and the formation multi π-stacks by the interaction with SWCNT stabilising the structure of the SWCNT/oligomer interphase [40].

On the other hand, the SWCNT is changed in its charged states by the interaction with a conducting polymer [41]. Using in situ Raman spectroelectrochemistry as the selective and sensitive method for the carbon nanotube structure [34, 35], the changes in a composite of semiconducting SWCNTs with the polymer poly(3,4-ethylendioxythiphene/polystyrenesulfonate) (PEDOT/PSS) were studied. The Raman spectra of the SWCNT-PEDOT/PSS composite correspond at a first glance to the superposition of the spectra of SWCNT and PEDOT/PSS, but the spectra are clearly dominated by the resonance-enhanced Raman lines of the SWCNT. It is obvious that already the mixing of SWCNT with PEDOT/PSS causes a partial doping of SWCNT as indicated by the change of the relative intensity of the Raman features of SWCNT. The in situ Raman spectroelectrochemical measurements (Fig. 11) clearly demonstrate that semiconducting tubes are doped even if they are embedded in PEDOT/PSS. However, in contrast to the neat SWCNT, the doping of SWCNT in composite is less efficient. Therefore, a larger potential (by about 0.4–0.6 V) is required to achieve the same doping level given by the bleaching of Raman bands as for neat SWCNT. By in situ Raman spectroelectrochemistry, it was thus demonstrated that the properties of the SWCNT/polymer composite are not a simple superposition of the properties of its

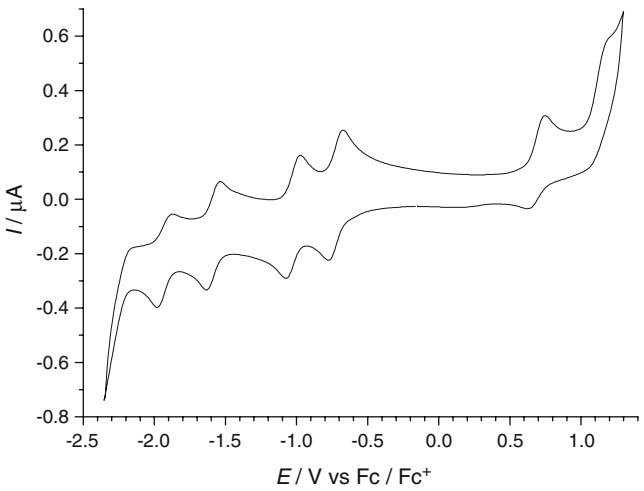

Fig. 12 Cyclic voltammogram of C_2–C_{82}:3 fullerene isomer in $TBAPF_6$/o-DCB solutions (potentials referred to the Fc/Fc^+ redox couple) [44]

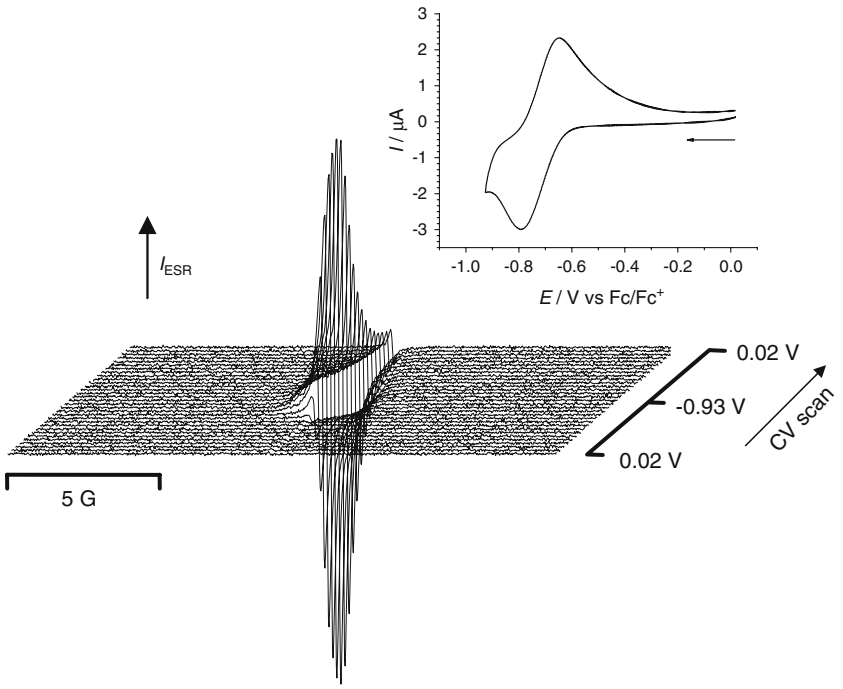

Fig. 13 Potential dependence of the ESR signal of the C_2–C_{82}:3$^{-\cdot}$ anion radical observed by in situ ESR spectroelectrochemistry. *Inset* Cyclic voltammogram of C_2–C_{82}:3 isomer in TBAPF$_6$/o-DCB solution for the first reduction [44]

components what is important for a precise control of the doping level.

Spectroelectrochemistry of carbon nanostructures in solution: the fullerenes

Like for carbon nanotubes, in situ Raman spectroelectrochemistry is also a preferred method for fullerenes especially in layers or other solid components [42]. By Raman spectroscopy, it was possible to clarify the state of C_{60} in electrochemically structured layers [42]. Nevertheless, for soluble carbon nanostructures, like fullerenes available in a molecular state in organic solvents (quite different from carbon nanotubes), it is the challenge to follow their electrode reaction in solution by a combined application of ESR and UV–vis NIR spectroscopy. In this way, it was possible to clarify the state of the C_{60} monoanion in organic solvents under electrochemical

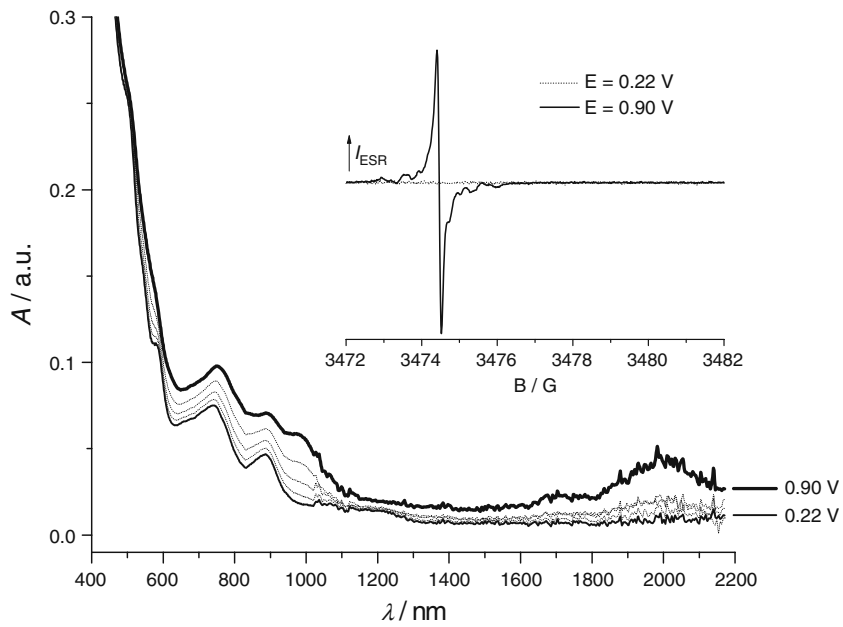

Fig. 14 UV/vis/NIR spectra of the C_2–C_{82}:3$^{+\cdot}$ cation radical observed during the anodic forward scan in in situ spectroelectrochemistry (*Inset*, ESR spectrum of the C_{82}:3$^{+\cdot}$ cation radical) [45]

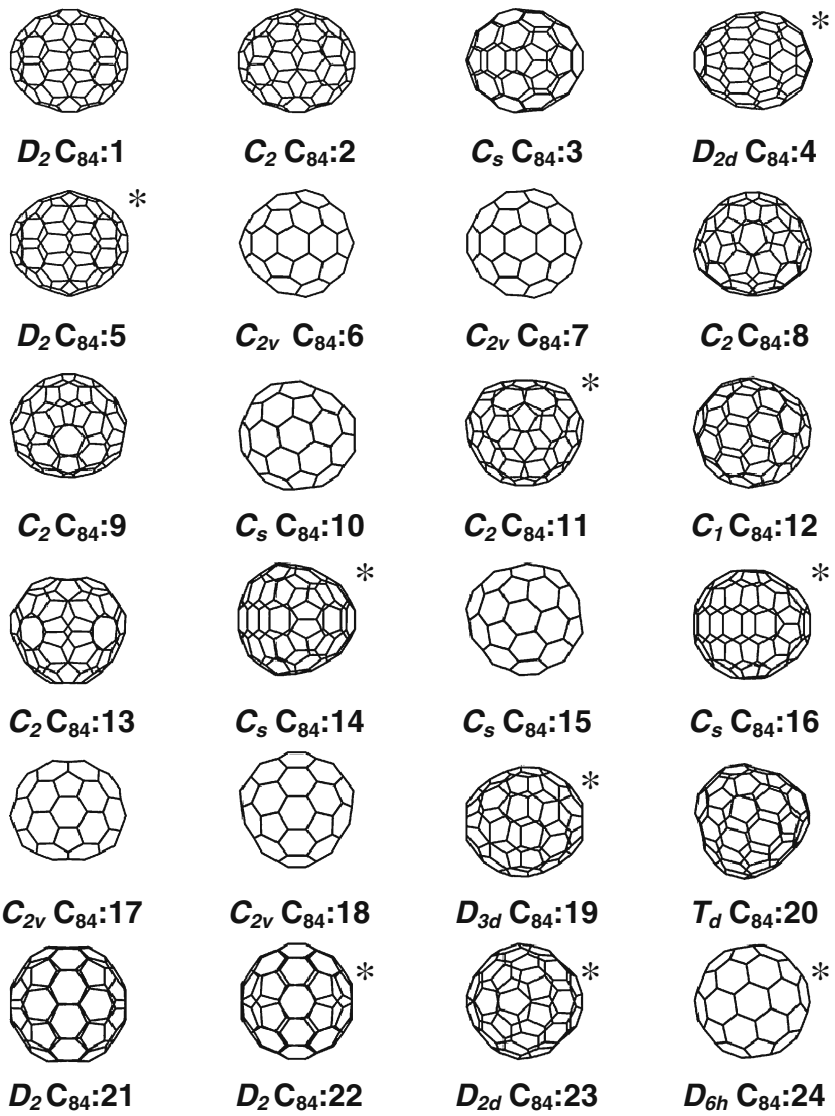

Fig. 15 The 24 IPR structures C_2–C_{82}: during the anodic forward scan in in situ spectroelectrochemistry (*Asterisk* denotes the preferred studied C_{84} isomer)

reduction [43]. The advantage of the two methods is demonstrated by the studies of different isomers of C_{84} and the behaviour of the most abundant isomer of C_{82}.

The increase of the fullerene cage size causes an increase in the number of stable cage isomers according to the isolated pentagon rule (IPR) but also a lowering of the oxidation potentials of large-size fullerenes, thus, being available for anodic reactions and the formation of positively charged fullerene cages in organic solvents like for C_{82} and C_{84} cages.

The C_{82} cage is the basis for a large variety of stable cage isomers in endohedral metallofullerenes for which the inclusion of different metal ions stabilises, e.g. the C_{3v} C_{2v} C_2 C_s isomers of C_{82} among the nine IPR obeying isomers. To understand the structure of endohedral C_{82} fullerenes with their charge separation of the endohedral metal and the fullerene cage, a detailed spectroelectrochemical study of the different anions and cations of an 'empty' cage C_{82} is required. The C_{82}:3 fullerene structure with C_2 symmetry is the most abundant isomer of C_{82} and, therefore, the best candidate for spectroelectrochemical studies [44–46].

The cyclic voltammogram of the C_2–C_{82}:3 fullerenes in o-DCB/TBAPF$_6$ solution (Fig. 12) points to four reversible reduction steps and two oxidation steps to be followed by in situ ESR UV–vis NIR spectroelectrochemistry [44, 45]. A very sharp ESR line (ΔB_{pp}=0.15 G) with a g-factor of 2.0009 and additional ^{13}C satellites is detected in the first reduction step for the monoanion (Fig. 13). In addition absorption bands of the monoanion with maxima at 670, 890, 1,135 and 1,850 nm are found by in situ UV–vis NIR spectroelectrochemistry (Fig. 13). Their potential dependence corresponds well with that of the ESR signal during the voltammetric cycle. Therefore, they can be assigned to the C_{82}:3 monoanion. The high degree of stability of the monocation is concluded from the reversible redox step in the cyclic voltammogram (Fig. 12). This made the ESR

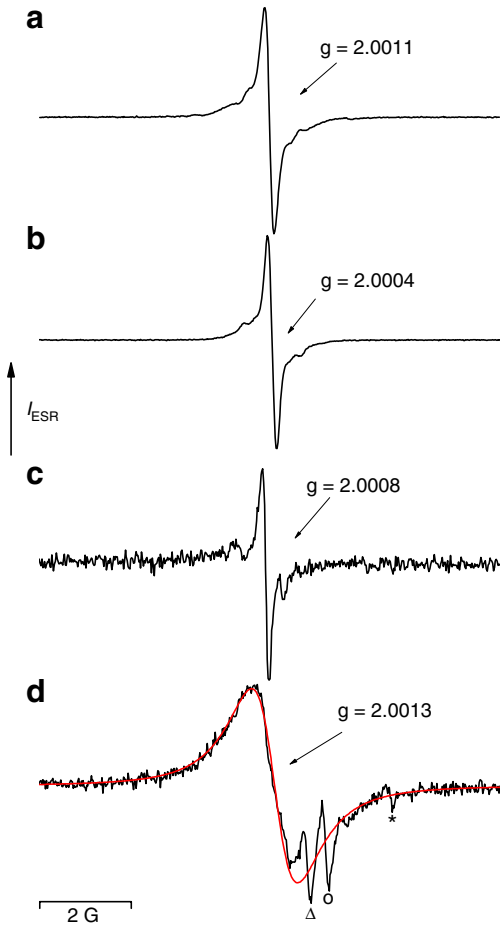

Fig. 16 ESR spectra of anion radicals of **a** C_{84}–C_s(14), **b** C_{84}–C_2(11), **c** C_{84}–D_2(22) and **d** C_{84}–D_{2d}(23) isomers detected by ESR spectroelectrochemistry at the first reduction step [47]

study of the cation radical of the C_2–C_{82}:3 isomer formed by anodic generation possible. Like for the monoanion, a very sharp ESR line (ΔB_{pp}=0.13 G) with ^{13}C satellites and a *g*-value of 2.0029 was observed for the cation radical. The ^{13}C satellite pattern is significantly different from the monoanion signal, pointing to a different spin distribution at the cage of the monocation. Two absorption bands at 890 and 1,995 nm are detected during the first oxidation step (Fig. 14). Their potential-dependent behaviour was that of the ESR signal and they can be clearly assigned to the C_{82}:3 cation radical. The absorption pattern was analysed by DFT calculations [47] and allows a clear description of the electronic state. It is important to point out that the NIR absorption maxima of fullerene cage as high as to around 2,000 nm requires the use of UV–vis NIR spectroelectrochemistry up to wavelengths of 2,000 nm and higher to get a complete characterization of the ionic states of fullerene ages. Therefore, modern in situ UV–vis NIR spectroelectrochemistry cover the range from 200 to 2400 nm in wavelength.

The electrochemistry of C_{84} fullerene isomers can demonstrate the power of ESR UV–vis NIR spectroelectrochemistry in many respects. As C_{84} is the third most abundant empty cage structure with 24 IPR isomers (Fig. 15), there are several cage structures available to be differentiated in their electronic structure in the ionic state. Based on extended high-performance liquid chromatography (HPLC) separations of individual isomers, the structures $C_s$$C_{84}$–$C_2$(11), C_{84}–C_s(14), C_{84}–D_2(22) and C_{84}–D_{2d}(23) were studied in detail, to get new insights in the electronic state of the C_{84} fullerenes with respect to the stability of these cage isomers in many endohedral fullerenes where the charge contributes essentially to the stability of the endohedral structure [47, 48].

The cyclic voltammetry of the four C_{84} isomers under study in *o*-DCB/TBAPF$_6$ solutions is in general similar to that of C_{82} (Fig. 12) but differing in the redox potentials of the single isomers and their electron-transfer steps. This difference is also obvious by the ESR spectra (Fig. 16) of C_{84}–C_2(11), C_{84}–C_s(14), C_{84}–D_2(22), and C_{84}–D_{2d}(23). While the low symmetric isomers C_{84}–C_s(14) and C_{84}–C_2(11) gives sharp singlet ESR lines (Fig. 16a, b) accompanied by ^{13}C satellites (ΔB_{pp}=0.20 G and *g*=2.0011 for C_{84}–C_s(14)) the third C_{84} fullerene isomer C_{84}–D_2(22) exhibits a sharp but not very intense ESR line (*g*=2.0008 ΔB_{pp}=0.17 G) with some sidebands (Fig. 16c). The reduction of the fourth C_{84} isomer C_{84}–D_{2d}(23) in the potential region of the first reduction step results in a quite complicated ESR spectrum consisting of at least three signals (Fig. 16d). The main broad ESR signal with a g-factor of 2.0013 and a linewidth ΔB_{pp}=1.00 G was attributed to the C_{84}–D_{2d}(23) monoanion. The minor impurity in the C_{84} monoanion ESR spectrum with a sharp line (ΔB_{pp} =0.15 G) and *g*=2.0009 which composes the 2% of the signal was identified as the monoanion of the C_{82}–C_2(3) isomer. The second impurity in the C_{84}–D_{2d}(23) is attributed to the C_{84}–C_s(16) isomer as these two isomers of C_{84} have very close retention times in HPLC. In this way, ESR spectroscopy turns out to be a powerful tool in the analysis of the purity of cage isomers of fullerenes via spectroelectrochemical electrochemical characterization. In general, ESR spectroelectrochemistry demonstrates that the symmetry of the fullerene molecule has a strong influence on the linewidth of the ESR signal of the monoanion decreasing with lower cage symmetry.

When expanding the potential range to the second reduction step, a decrease in the intensity of the monoanion ESR line was observed for all isomers as illustrated for C_{84}–C_s(14) isomer (Fig. 17a). The diamagnetic dianions formed in the second reduction step are to be followed by vis-NIR spectroelectrochemistry. Here, new optical bands at 835, 1,147 and around 1,850 nm appear in the second reduction step (Figs. 17b, 4a green line). These bands can be assigned to the C_{84}–C_s(14) dianion based on the

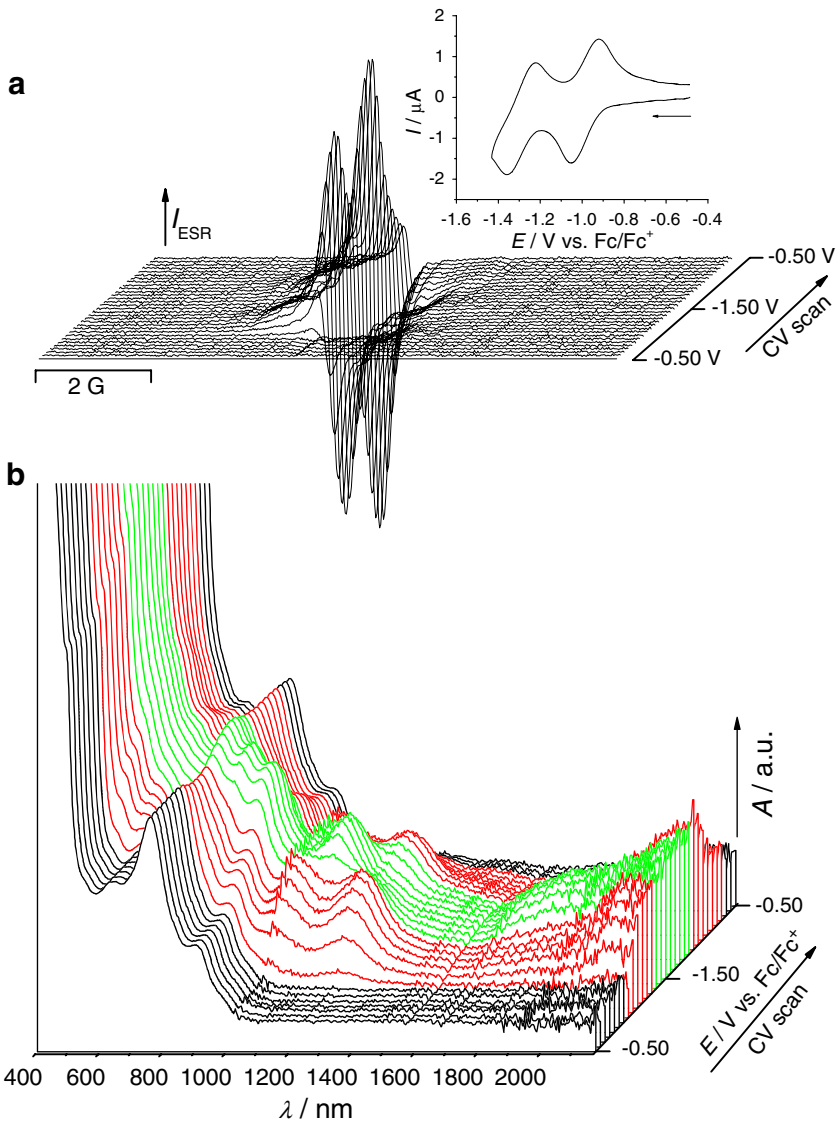

Fig. 17 **a** Potential dependence of the ESR spectra of C_{84}–C_s(14) detected in the first and second reduction step. (*Inset*, cyclic voltammogram at the frist two reduction steps) **b** Potential dependence of the Vis/NIR spectra of C_{84}–C_s(14) in the first and second reduction step; neutral, *black lines*; monoanion, *red lines*; dianion, green lines [48]

correlation of their intensities with the charge transferred in the second reduction step.

During the reduction of the C_{84}–C_s(14) isomer at the third reduction step, a new ESR signal with a g-factor of 2.0015 and a linewidth of ΔB_{pp}=0.18 G appeared (Fig. 18a). This new signal can be assigned to the C_{84}–C_s(14) trianion according to the correlation of its intensity with the third reduction and re-oxidation peaks in cyclovoltammetric trace. The new ESR signal is partially overlapped by that of the monoanion but the subtraction of the monoanion signal results in the ESR spectrum of the C_{84}–C_s(14) trianion which significantly differ in its ^{13}C satellite pattern (Fig. 18b). In the fourth reduction step of C_{84}–C_s(14), a decrease of the trianion ESR signal is observed pointing to the diamagnetic state of the tetraanion of the C_{84}–C_s(14) fullerene. A larger separation in g-factors between the signals of the mono- and trianion was observed for the C_{84}–C_2(11) isomer and again the ^{13}C satellite patterns are different for the singly and triply charged fullerene (Fig. 18c).

Summarising the fullerene isomer study, in situ ESR vis NIR spectroelectrochemistry turns out to be the matter of choice for the C_{84} isomers C_{84}–C_2(11), C_{84}–C_s(14), C_{84}–D_2(22) and C_{84}–D_{2d}(23) as examples for the large variety of fullerene isomers to characterise the electronic situation of their neutral and negatively charged states.

How different the electronic situation in a fullerene structure might be in dependence on charging will be demonstrated with the example of in situ ESR Vis NIR spectroelectrochemistry of the endohedral derivative $Sc_3N@C_{80}(CF_3)_2$ which exhibits three reversible reduction and two reversible oxidation steps [49]. The monocation,

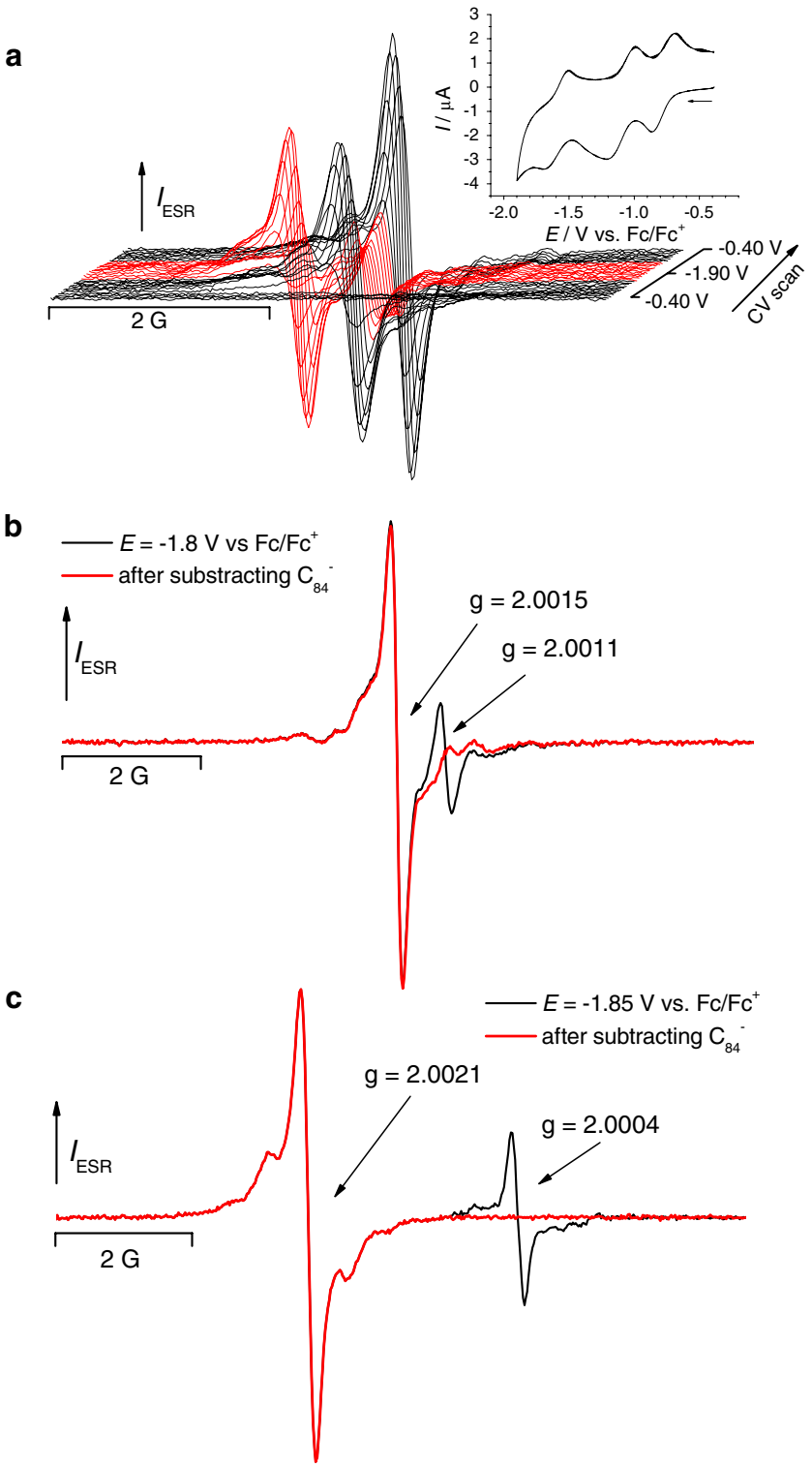

Fig. 18 **a** The potential dependence of ESR spectra of C_{84}^{-}–$C_s(14)$ and C_{84}^{3-}–$C_s(14)$ in the potential region of the first, second and third reduction step. (*Inset* cyclic voltammogram), **b** ESR spectrum of C_{84}^{3-}–$C_s(14)$ overlapped by the signal of C_{84}^{-}–$C_s(14)$ (*black line*) and after C_{84}^{-}–$C_s(14)$ signal subtraction (*red line*) and **c** ESR spectrum of C_{84}^{3-}–$C_2(11)$ with the signal of C_{84}^{-}–$C_2(11)$ (*black line*) and after C_{84}^{-}–$C_2(11)$ signal subtraction (*red line*) [48]

the monoanion and the trianion are available by ESR spectroscopy in solution, providing for the first time a broad range of spectroscopically available charged states of an endohedral fullerene via spectroelectrochemistry. The addition of two CF_3 groups to a $Sc_3N@C_{80}$ endohedral structure dramatically changes the spin density distribution upon charging. The DFT analysis of the ESR spectra of the monoanion and the trianion indicates a spin-density shift from the fullerene cage to the Sc_3N cluster upon charging resulting in a high spin density on one Sc atom in the trianion (Fig. 19). Therefore, in complex fullerene structures, it is the spin density distribution which can be varied

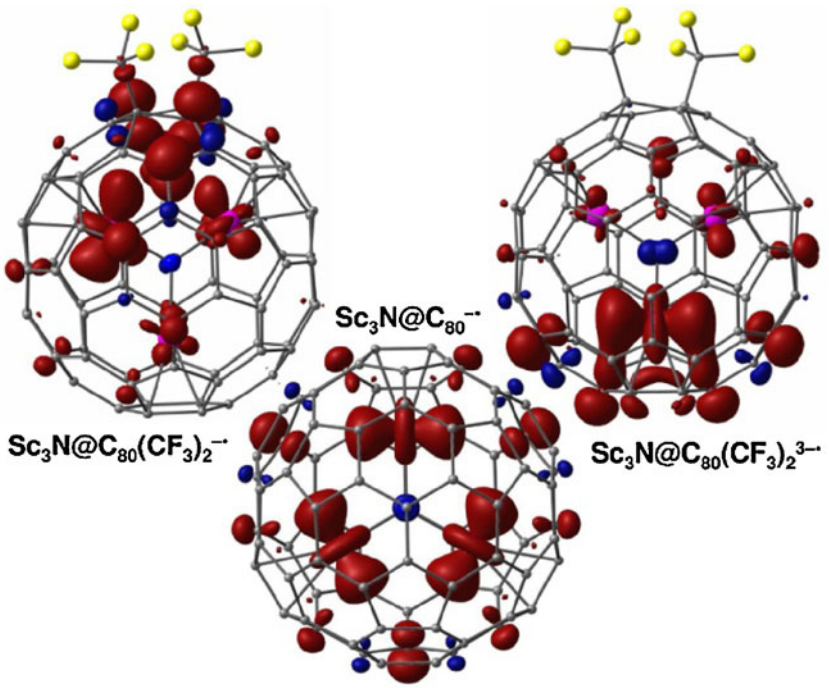

Fig. 19 DFT computed spin density distribution in the lowest energy conformers of monoanion $Sc_3N@C_{80}(CF_3)_2^-$ (*top left*), the trianion $Sc_3N@C_{80}(CF_3)_2^{3-}$ (*top right*) and the non-derivatised monoanion $Sc_3N@C_{80}^-$ (*middle bottom*) [49]

by charging of selected fullerenes structure. This opens new insights into endohedral fullerene structures enabled by spectroelectrochemistry.

The future

As demonstrated in this review, a general trend in spectroelectrochemistry is under way from single spectroelectrochemical towards multi-spectrolectrochemcial techniques. There is no doubt that further progress in spectroscopic techniques will result in a variety of triple methods like in situ ESR UV–vis NIR spectroelectrochemistry to make a more detailed structural characterisation of electrode systems and reaction mechanisms possible. Nevertheless, strong efforts are required to develop spectroelectrochemical setups for such triple methods to ensure the accuracy of the electrode potential control and the sensitivity of the spectroscopic methods. While this future work is an obvious consequence of the current developments in spectroscopy, there are further aspects which require a new technical breakthrough. Especially, the time resolution in spectroelectrochemistry must be turned to a new dimension of time scale to fulfill the requirements of current developments in electrochemistry as it is, e.g. the field of endohedral electrochemistry [50]. Here, the pathway of the endohedral electron transfer at the fullerene cage is to be followed experimentally at a time scale beyond the current available range.

Furthermore, locally resolved spectral information of an electrode surface is the matter of choice to get the distribution of chemical structure under dynamic conditions of an electrode reaction. Currently, Raman spectroscopy is the most developed spectroscopic method in this field [51], but there is no doubt that other spectroscopic techniques might reach a high standard of spatial resolution as well. It is obvious that for the phase boundary of an electrode, it is of high importance to follow the gradients of chemical species under reaction conditions. Therefore, the application of any type of spectral imaging will have a great chance in electrochemistry as far as the spatial resolution is in the range of the extension of the (diffuse) electrochemical double layer and sufficient for an analysis of the diffusion in the concentration layer at both sides of the electrode interface.

In general, it is a great challenge for experimental electrochemists in the next future to contribute to modern electrochemistry with outstanding developments in experimental methods—because of and beyond the main stream of charge storage systems or fuel cells.

Acknowledgements For scientific cooperation, the author would like to thank Dr. Evgenia Dmitrieva, Dr. Kinga Haubner, Dr. Sabrina Klod and Dr. Alexey Popov (all of IFW Dresden) as well as Dr. Vladimier Lukes, Doc. Dr. Peter Rapta, Dr. Michal Zalibera (all of STU Bratislava), Prof. Ladislav Kavan and Dr. Martin Kalbac (both of JHI, Prague) and Dr. Jan Tarabek (IOBC Prague). Technical support by Sandra Schiemenz, Marco Rosenkranz and Frank Ziegs (all of IFW Dresden) is gratefully acknowledged. The research was supported by

grants from Humboldt foundation, DFG and BMBF which are duly acknowledged.

References

1. Bard AJ, Faulkner LR (2001) Electrochemical methods—fundamentals and applications, 2nd edn. Wiley, New York
2. Rossiter BW, Hamilton JF (eds) (1986) Physical methods of chemistry, vol 2. Electrochemical Methods Wiley, New York
3. Bamford CH, Compton RG (eds) (1986) Chemical kinetics vol. 26. Elsevier, Amsterdam
4. Southampton Group (ed) (1990) Instrumental methods in electrochemistry, 2nd edn. Chichester, Ellis Horwood
5. Bond AM (2002) Broadening electrochemical horizons. University Press, Oxford
6. Marken F, Neudeck A, Bond AM (2009) Cyclic voltammetry. In: Scholz F (ed) Electroanalytical methods: guide to experiments and applications, 2nd edn. Springer, Berlin, pp 57–106
7. Abruna HD (ed) (1991) Electrochemical interfaces. Modern techniques for in situ interface characterization. VCH, New York, Weinheim
8. Kaim W, Klein A (eds) (2008) Spectroelectrochemistry. Royal Society, London
9. Plieth W, Wilson GS, Gutierrez De La Fe CG (1998) Pure Appl Chem 70:1395–1414
10. Furtak TE, Kliewer KL, Lynch DW (eds) (1980) Non-traditional approaches to the study of the solid-electrolyte interface. Elsevier, Amsterdam
11. Hansen WN, Kolb DM, Lynch DW (eds) (1983) Electronic and molecular structure of electrode-electrolyte interfaces. Elsevier, Amsterdam
12. in situ characterization of electrochemical processes (1987) (NMAB-Publikation 438–3) ACS, Washington/DC
13. Gale RJ (ed) (1988) Spectroelectrochemistry. Plenum, London and New York
14. Compton RG, Hamnett A (1989) New techniques for the study of electrodes and their reactions, comprehensive chemical kinetics vol. 29. Elsevier, Amsterdam
15. Gutierrez C, Melendres C (eds) (1990) Spectroscopic and diffraction techniques in interfacial electrochemistry Kluwer, Dordrecht
16. Varma R, Selman JR (eds) (1991) Techniques for characterization of electrodes and electrochemical processes. Wiley, New York
17. Lipkowski J, Ross PN (eds) (1993) Structure of electrified interface. VCH, New York, Weinheim, Wellington
18. Alkire RC, Kolb DM, Lipkowski J, Ross PN (eds) (2006) Diffraction and spectroscopic methods in electrochemistry (Advances in electrochemical science and engineering vol. 9). Wiley-VCH, Weinheim
19. Winterbottom AB (1946) Trans Faraday Soc 42:487–495
20. Winograd N, Blount HN, Kuwana T (1969) J Phys Chem 73:3456
21. Austen DEG, Given PH, Ingram DJE, Peover ME (1958) Nature 182/4652:1784–1786
22. Maki AH, Geske DH (1959) J Chem Phys 30:1356–1357
23. Goldberg IB, Bard AJ (1971) J Phys Chem 75:3281–3290
24. Kuwana T, Darlington RK, Leedy DW (1964) Anal Chem 36:2023–2025
25. Hansen WN, Horton JA (1964) Anal Chem 36:783–786
26. Heinemann WR, Burnett JN, Murray RW (1968) Anal Chem 40:1974–1978
27. Fleischmann M, Hendra PJ, McQuilla AJ (1974) Chem Phys Lett 26:163–166
28. Richards JE, Evans DH (1975) Anal Chem 47:964–966
29. Klod S, Ziegs F, Dunsch L (2009) Anal Chem 81:10262–10267
30. Fleischmann M, Oliver A, Robinson J (1986) Electrochim Acta 31:899–906
31. Samant MG, Toney MF, Borges GL, Blum L, Melroy OR (1988) Surf Sci 193:L29–L36
32. Petr A, Dunsch L, Neudeck A (1996) J Electroanal Chem 412:153–158
33. Sturm J, Künzelmann U, Bischoff S, Dunsch L (1996) Bruker Report 142:8–11
34. Kavan L, Dunsch L (2007) ChemPhysChem 8:975–998
35. Kavan L, Dunsch L (2011) ChemPhysChem 12:47–55
36. Haubner K, Tarabek J, Ziegs F, Lukes V, Jähne E, Dunsch L (2010) J Phys Chem 114:1545–11551
37. Klod S, Haubner K, Jähne E, Dunsch L (2010) Chem Sci 1:743–750
38. Dmitrieva E, Harima A, Dunsch L (2009) J Phys Chem 113:16131–16141
39. Kellenberger A, Dmitrieva E, Dunsch L (2011) PhysChemChemPhys 13:3411–3420
40. Haubner K, Luspai K, Rapta P, Dunsch L (2011) PhysChemChemPhys, doi:10.1039/c1cp20738e
41. Kalbac M, Kavan L, Dunsch L (2009) Synth Met 159:2245–2248
42. Krause M, Deutsch D, Janda P, Kavan L, Dunsch L (2005) PhysChemChemPhys 7:3179–3184
43. Rapta P, Bartl A, Gromov A, Staško A, Dunsch L (2002) ChemPhysChem 3:351–356
44. Zalibera M, Rapta P, Dunsch L (2007) Electrochem Comm 9:2843–2847
45. Zalibera M, Popov AA, Kalbac M, Rapta P, Dunsch L (2008) Chem Eur J 14:9960–9967
46. Solc R, Lukes V, Ilcin M, Rapta P, Zalibera M, Dunsch L (2009) J Phys Chem 113(45):19658–19663
47. Zalibera M, Rapta P, Dunsch L (2008) Electrochem Comm 10:943–946
48. Zalibera M, Rapta P, Popov AA, Dunsch L (2009) J Phys Chem 113:5141–5149
49. Popov AA, Shustova NB, Svitova AL, Mackey MA, Coumbe CE, Philips JP, Stevenson S, Strauss SH, Boltalina OV, Dunsch L (2010) Chem Eur J 16:4721–4724
50. Popov AA, Dunsch L (2011) J Phys Chem Lett 2:786–794
51. Pettinger B (2010) Mol Phys 108:2039–2059